

*Region-Specific Correlations Between  $\|V_{\mathbf{S}30}\|$  and Time-Averaged  $V_{\text{S}}$  and SPT-N Values at Different Depths for the Indo-Gangetic Basin*

**P. Anbazhagan & Ketan Bajaj**

**Indian Geotechnical Journal**

ISSN 0971-9555

Volume 50

Number 3

Indian Geotech J (2020) 50:454-472

DOI 10.1007/s40098-019-00379-1

**Your article is protected by copyright and all rights are held exclusively by Indian Geotechnical Society. This e-offprint is for personal use only and shall not be self-archived in electronic repositories. If you wish to self-archive your article, please use the accepted manuscript version for posting on your own website. You may further deposit the accepted manuscript version in any repository, provided it is only made publicly available 12 months after official publication or later and provided acknowledgement is given to the original source of publication and a link is inserted to the published article on Springer's website. The link must be accompanied by the following text: "The final publication is available at [link.springer.com](http://link.springer.com)".**



# Region-Specific Correlations Between $V_{S30}$ and Time-Averaged $V_S$ and SPT-N Values at Different Depths for the Indo-Gangetic Basin

P. Anbazhagan<sup>1</sup> · Ketan Bajaj<sup>1</sup>Received: 26 October 2018 / Accepted: 15 July 2019 / Published online: 25 July 2019  
© Indian Geotechnical Society 2019

**Abstract** Time-average shear wave velocity at top 30 m depth ( $V_{S30}$ ) is extensively used for site characterization and amplification parameters estimation. However, due to various reasons, the shear velocity profile ( $V_S$ ) does not reach to 30 m depth. In this study, using the multichannel analysis of surface waves,  $V_S$  profiles at 275 locations have been determined in the Indo-Gangetic Basin (IGB). Further using  $V_S$  profiles, new correlations between  $V_{S30}$  and  $V_{SZ}$  (where  $z$  is the average depth) have been developed for  $z < 30$  and  $z > 30$  m. For  $z < 30$ , second degree polynomial equation has been used for deriving  $V_{S30}$  and  $V_{SZ}$  correlation for  $z$  ranging from 5 to 29 m in 1 m increment. Whereas for  $z > 30$ , both linear and second-order polynomial equations have been used. Based on the variation of residual with  $V_{S30}$ , it has been observed that second-order polynomial equation derived using orthogonal regression is performing better in both cases. Additionally, new correlations between  $V_{S30}$  and SPT- $N_z$ , with  $z$  equals to 5, 10, 20, 30, 40 and 50 m, have been derived. This correlation is further used in deriving the  $N_{30}$  map of the IGB as per BIS:1893 useful for Indian scenario. Further, the depth corresponding to one-quarter of wavelength for various periods has been studied. The velocities known up to 30 m depth are relevant for site amplification at period up to 0.5 s. This is the first time such extensive study has been carried out in the IGB for correlation of  $V_{S30}$  and  $V_{SZ}$ , for both deep and shallow depths.

**Keywords** MASW ·  $V_{S30}$  ·  $V_{SZ}$  · SPT-N · Orthogonal regression · Site amplification

✉ P. Anbazhagan  
anbazhagan@iisc.ac.in

<sup>1</sup> Department of Civil Engineering, Indian Institute of Science, Bangalore 560012, India

## Introduction

The Indo-Gangetic Basin (IGB) is the largest alluvial tract of Ganga, Indus and Brahmaputra rivers and their tributaries in the world, which is formed in response to the Himalayan orogeny. Active sedimentation and neotectonic activities result in the deposition of different layers of soil at various parts of the IGB. Geological Society of India (GSI) has reported that in some parts of the IGB the Quaternary alluvium lies unconformably over the basement comprising Bundelkhand Granites and sedimentary rocks of the Vindhyan super group. Additionally, depth of bedrock varies from 298 to 445 m, respectively, in the southern and western parts; however, in the northeastern part, the depth of bedrock is not encountered up to a depth of 637 m. GSI has recognized different landform and surface (i.e., Siwalik uplands, Newer and older Alluvium) along the entire stretch of IGB. Hence, the spatial variability of dynamic property, i.e., shear wave velocity is highly required in the entire stretch of the IGB.

Shear wave velocity is a vital factor for site characterization and site effect assessment. However, time-average shear wave velocity up to 30 m ( $V_{S30}$ ) depth has considered in various earthquake geotechnical engineering applications.  $V_{S30}$  has been explicitly used as site effect parameter in ground motion prediction equation in NGA-West 2 project, and it is the basis of seismic site classification [1–3]. Even though  $V_{S30}$  can be obtained at a reasonable cost, it cannot apprehend the physical condition that controls the site amplification [4, 5].  $V_{S30}$  was a practical choice initially, even nowadays  $V_{S30}$  is widely used and a number of  $V_{S30}$  data are extremely high [6]. However,  $V_{S30}$  has lot of limitations, like getting the complete shear wave velocity ( $V_S$ ) profile until the bedrock is often difficult and expensive for low-budget projects. There are various

instruments and techniques available for estimating the  $V_S$  profile at a given site. However, for a number of reasons,  $V_S$  could not reach to 30 m depths, which was pointed out by Boore et al. [7] and Boore [8]. One crude way to resolve this issue is to derive  $V_{S30}$  using the corresponding bore log data for which bottom depth of more than 30 m is known. The other way is to determine the relationship between  $V_{S30}$  and time-average shear wave velocity up to different depths ( $V_{SZ}$ ). Various authors [6–9] derived the correlation between  $V_{S30}$  and  $V_{SZ}$ . Various researchers have made an effort to develop the site classification map of different parts of India. Anbazhagan and Sitharam [10], Mahajan et al. [11], Maheshwari et al. [12], Satyam and Rao [13] and Anbazhagan et al. [14] have developed shear wave velocity map of Bangalore, Dehradun, Chennai, Delhi and Lucknow, respectively. Similarly, Govindaraju and Bhat-tacharya [15], Hanumantha Rao and Ramana [16], Phani-kanth et al. [17], Shukla and Choudhary [18], Desai and Choudhary [19] have determined the  $V_S$  for carrying out the site response study for Kolkata, Delhi, Mumbai, Gujarat and Mumbai, respectively. However, these studies are restricted up to shallow depths, i.e., 30 m, and no extensive study has been done for correlating  $V_{SZ}$  and  $V_{S30}$ , of entire IGB or any region in India.

In this study, a combined active and passive multi-channel analysis of surface wave (MASW) survey has been used for determining the shear wave velocity ( $V_S$ ) profile at 275 locations in the entire IGB. Using these  $V_S$  profiles, new correlations between  $V_{SZ}$  and  $V_{S30}$  with  $z < 30$  and  $z > 30$  have been developed. Based on the geological and velocity variability, the IGB is divided into three regions, i.e., Punjab–Haryana Region (PHR), Uttar Pradesh Region (UPR) and Bihar Region (BR). Separate correlation between  $V_{SZ}$  and  $V_{S30}$  has been derived using both least square and orthogonal analysis. For depth less than 30 m, correlation between  $V_{SZ}$  and  $V_{S30}$  has been derived using second-order polynomial equation at an interval of 1 m from 5 to 29 m for the IGB. For depth more than 30 m, suitability of both second-order polynomial equation and linear equation has been tested using variation of residuals with  $V_{S30}$ . As in many sites in India, a correlation between  $V_S$  and SPT-N has been widely used. However, these correlations do not predict  $V_{S30}$  directly, also when  $V_S$  or  $N$  data are available for less than 30 m,  $V_{S30}$  value estimation using extrapolated values may lead to error. So, additionally, new correlations between  $V_{S30}$  and SPT- $N_z$ , with  $z$  equals to 5, 10, 20, 30, 40 and 50 m, have been derived for IGB using available bore log. The average SPT-N value up to the depth of 30 m ( $N_{30}$ ) value is suggested in BIS:1893 [20] for site classification; hence,  $N_{30}$  map has been generated considering correlation between  $N_{30}$  and  $V_{S30}$ . Further, the depths corresponding to one-quarter of wavelength for various periods have been studied. The

velocities known up to 30 m depth are relevant for site amplification at period up to 0.5 s. This is the first time, correlation between  $V_{SZ}$  and  $V_{S30}$  has been studied extensively for deep basins of IGB.

## Study Area

The IGB is the immense plain of Ganga and Indus River and their tributaries, including the most populous portion of India. IGB is formed in response to the Himalayan orogeny. It shows all the major components of a foreland basin, namely orogen (the Himalaya), deformed and uplifted foreland basin deposits adjacent to orogen (Sivalik hills), a depositional basin (Ganga Plain), and peripheral cratonic bulge (Bundelkhand-Vindhyan Plateau) [21]. Strong asymmetry in the depth of soil deposit has been reported by various researchers [21, 22] along the entire stretch of IGB. Deposition depth varies from 0.5 to 1 km in its southward and 6–8 km in its Northwards near to Sivalik hills and thins out as a mere veneer on the Peninsular margin.

The present study area is a part of the Himalayan foreland basin, lies roughly between longitude 74°E and 88°E and latitude 24°N and 32°N (See Fig. 1). The Ganga foreland basin originated in the early Miocene and from middle Miocene to middle Pleistocene, and the northern part of the IGB was uplifted and thrust basin wards and the Ganga plains shifted southwards in response to thrust loading in the orogen [21]. The soil deposit in the study area can be broadly classified into Older and Newer alluvium. The former consists of beds, which are undergoing denudation and the latter from floods and delta deposits is now in process of formation. The older alluvium is composed of massive beds of clay of pale reddish-brown color. However, newer alluvium consists of coarse gravel near the base of the Himalaya, sand clay and sand in the proximity of the river channels, and fine silt consolidating into clay in the flatter parts of the river plains and the deltas (Geological Society of India, [www.gsi.gov.in](http://www.gsi.gov.in)).

Based on geological, tectonic and geomorphology, the study area is further divided into three parts, i.e., Punjab–Haryana Region (PHR), Uttar Pradesh Region (UPR) and Bihar Region (BR). PHR chiefly forms the part of Indus basin with the Satluj, Beas and Ravi rivers joining the Indus River. Most of the area of PHR is occupied by the Quaternary deposits, which can be classified into (a) Newer Alluvium (b) Older Alluvium and (c) Eolian deposits. Except for the northeastern part of Punjab, in the Siwalik foothills, the area is occupied by the Quaternary sediments. The thickness of the alluvium in this area is up to 4.5 km [21], deeper in the northwestern and northern Punjab and thinner on the southern side. Karunakaran and Rao [23] reported the presence of Palaeozoic, Mesozoic and Tertiary

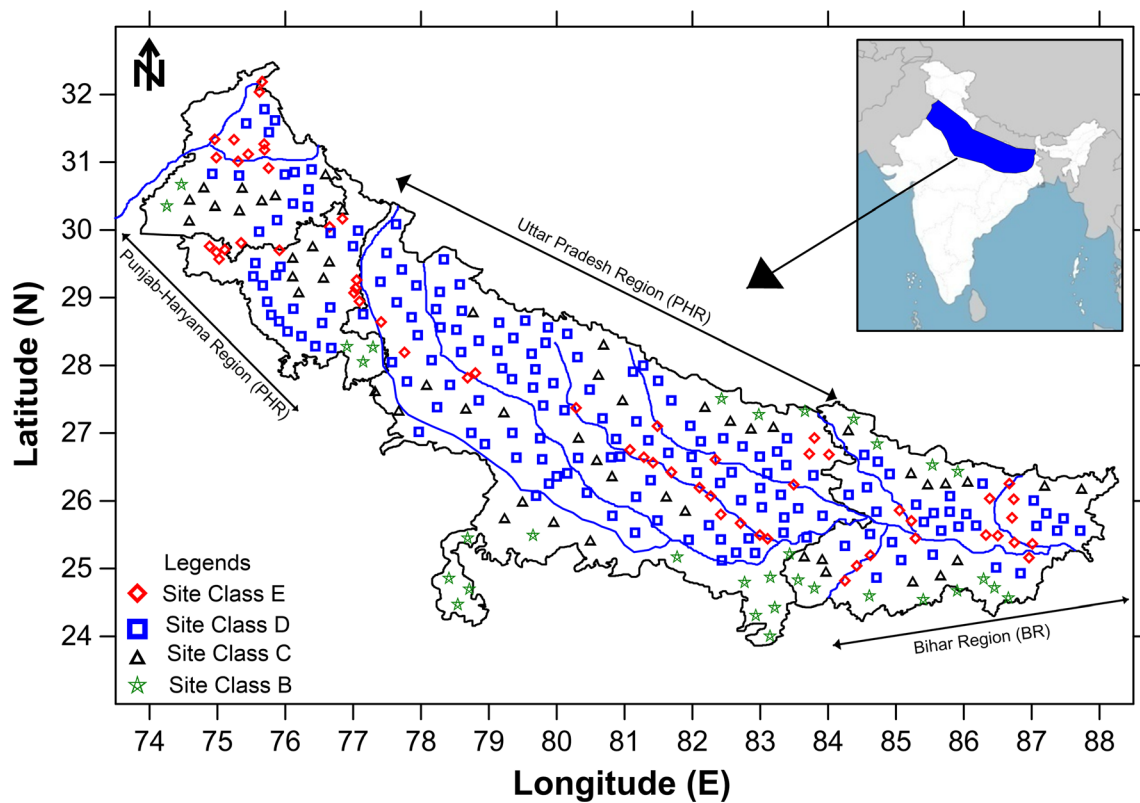


**Fig. 1** Location of MASW survey along the entire stretch Indo-Gangetic with seismic site classification as per NEHRP

formation below; however, the alluvium is chiefly underlined by Siwalik sediments. Haryana is covered by Quaternary eolian and alluvium deposit, which unconformably overlie the quartzites and granites of the Delhi supergroup, Nagpur sandstone of Cambrian age and tertiary clays [24]. Geology of UPR is occupied by diverse rocks types ranging from Archaean metamorphites/granitoids to the youngest Quaternary alluvium. Depending on the lithology, the Quaternary sediments have been broadly classified into Banda older alluvium (BOA), Varanasi older alluvium (VOA) and Newer alluvium. BOA is exposed in the south of Yamuna River and rest over Precambrian rocks. VOA consists of polycyclic sequence of brownish silt clay and micaceous sand and overlies over the BOA. Newer alluvium represents the youngest sequence and is confined with the flood plain area of UPR. Additionally, UPR is moderately seismically active, and earthquakes are caused due to the release of part of strains away from the plate boundary. Khan et al. [25] discussed the activity of the ten cross-faults along this region and concluded that most of them are active. About half of the area of the BR is occupied by the Quaternary sediments of recent to sub-recent age and also tectonically active. The Quaternary alluvium of BR is unconformably overlying the basement composed of the Gondwana, Vindhyan and Pre-Vindhyan formation. Depth of basement varies from 1000 m in

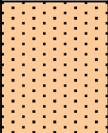
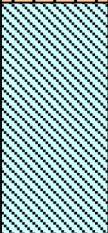
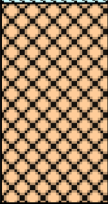
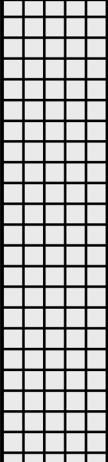
marginal alluvium plain to 5000 m near to the Siwalik foothills [21, 22]. BR basement is occupied by various faults, ridges and depressions, of which Munger Saharsa fault, east Patna fault and west Patna fault are reported as most active fault [26]. Typical bore log of study area is given as Fig. 2. The detailed description of geology of the IGB is given in Bajaj and Anbazhagan [27, 28].

### Field Data Acquisition and Analysis

Multichannel analysis of surface wave (MASW) is used for estimating the shear wave velocity ( $V_S$ ) profile for shallow and deeper depths for IGB. MASW emphasized on the minimization of nearfield and far-offset effects, sampling redundancy, acquisition speed, and overall data accuracy [29]. The variation of  $V_S$  in a layered medium is estimated using the inversion of the dispersion curve of surface wave via MASW [29–31]. Xia et al. [30] showed the dependency of  $V_S$  on dispersion of the Rayleigh wave of the subsurface layered material. However,  $V_S$  estimated from dispersion curve derived from surface wave, mainly depends on scattered and non-source-generated surface waves, source-generated noises (i.e., body wave) and higher-mode surface wave [29]. Additionally, frequency of waveforms and distance from the source governs the interference of noises in the dispersion curve. It can be separated considering the

**Fig. 2** Typical bore log of study area

(a)

Location	PHR	Date	15-01-2015		
Depth Below GL (m)	Soil Description	Thickness of layer (m)	Legend	SPT-N value	
0	Silt	2		10	
1				12	
2		3			15
3					17
4	23				
5	Clay with Kankar	6		23	
6					
7					
8					
9					
10					
11	Grey Fine Grained Sand	13		25	
12				23	
13				28	
14				30	
15					
16				35	
17					
18					
19					
20					
21					
22					
23					
24					
25					
26					
27					
28					
29					
30					

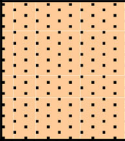
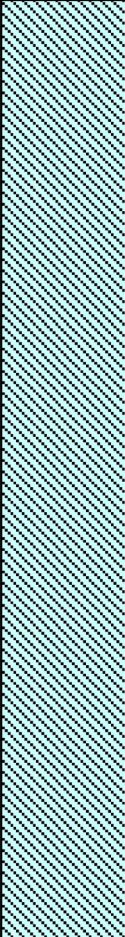
coherency in arrival time and amplitude in MASW [29, 30].


MASW operates the three-step standard algorithm in surface wave assessment, i.e., (1) accruing the raw experimental data; (2) processing the signal/data to obtain experimental dispersion curve; (3) solve the inverse problem to estimate the modal parameters. Both active and passive source can be used in the recording of the surface wave. When the artificial energy source (i.e., sludge hammer) is employed in surface wave recording, it is called as active MASW survey, whereas when energy source is ambient noise (i.e., traffic or tidal waves), it is called as passive MASW survey. In case of active method, the investigation depth is usually shallower than 30 m, whereas it can reach a few hundred meters with the passive method. This may be owing to the limitation that arises at

low frequencies in active data. Most of the critical structures (e.g., site amplification for Nuclear Power Plant, Dam, etc.) requires  $V_s$  for deeper depths, which can be attained either from broadband sensors or from heavy energy source in case of active MASW. Such sources are not only expensive but also uncontrollable in filed operation, because of uncertainty in its operation. To resolve this many investigators are using passive surface waves from natural (e.g., tidal, atmospheric) and cultural (e.g., traffic) origins and get the frequencies lower up to 1 Hz [32]. However, to get the dispersion at lower frequencies, passive MASW method requires 2D receiver array, which is difficult in densely populated area. To overcome this, Park and Miller [33] proposed a passive MASW along the roadside, which is used in this study to get dispersion curve at low frequencies and  $V_s$  profile at deeper depths.

Fig. 2 continued

(b)

Location	UPR	Date	22-05-2005	
Depth Below GL (m)	Soil Description	Thickness of layer (m)	Legend	SPT-N value
0	Silty Clay	3		8
1				
2				
3				
4	Clayey Silt	27		13
5				
6				
7				
8				
9				
10				
11				
12				
13				
14				
15				
16				
17				
18				
19				
20				
21				
22				
23				
24				
25				
26				
27				
28				
29				
30				

 GW

These MASW methods are widely used to estimate the  $V_S$  of the near-surface materials [e.g., 29, 31, 33, 34]. In this study, active and passive data are recorded at same site to get the dispersion curve at different frequency bands. For investigating  $V_S$ , Park et al. [35] used the active and passive MASW, respectively, for frequency less than 30 and more than 30. Merging both the dispersion curve enhances the overall nature in extended frequencies and phase velocity ranges, resulting in more effective  $V_S$  profile of a site [28, 35]. The comparison and validation of the obtained  $V_S$  with lithology and SPT-N value can be referred from Bajaj and Anbazhagan [28]. It can be also noted here that Anbazhagan et al. [36] presented

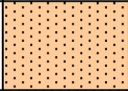


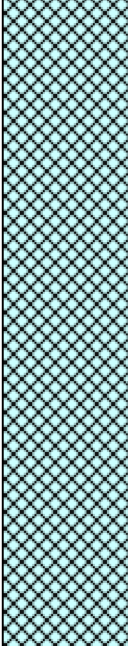
parametric study on passive data acquisition and analysis to arrive at suitable field and recording parameters to get reliable  $V_S$  profile in IGB

**Data Acquisition and Analysis**

Two hundred and seventy-five MASW surveys have been done in the entire stretch of IGB by dividing it into three parts, i.e., PHR, UPR and BR, as shown in Fig. 1. Out of 275, 75, 130 and 70 MASW surveys have been done, respectively, in PHR, UPR and BR. Approximately MASW testing area covered is about 250,000 km<sup>2</sup> of IGB. Both active and passive MASW surveys have been done at each

Fig. 2 continued

(c)

Location	BR	Date	09-08-2008	
Depth Below GL (m)	Soil Description	Thickness of layer (m)	Legend	SPT-N value
0	Silty Clay	2		9
1				
2				
3	Clay with high plasticity	3		13
4				
5				
6	Clay with intermediate plasticity	3		19
7				
8				
9	Silt of intermediate plasticity	22		22
10				
11				
12				
13				
14				
15				
16				
17				
18				
19				
20				
21				
22				
23	32			
24				
25				
26				
27	36			
28				
29				
30				

GW

location to get dispersion curve at both low and high frequencies. Test setup consists of 24 channel Geode seismographs in combination with 24 vertical geophones of 2.0 Hz frequency. For an active survey, an impulsive source of 10 kg sledgehammer striking against a 30 cm × 30 cm size steel plate generates surface waves. For getting the active and passive data, geophones spacing were varied from 3 to 5 m depending on the availability of the space. For active data recording, the shot locations (i.e., the distance between the source and the first geophone) were varied from 3, 6 and 10 m. To enhance the active MASW data, at each location 5, multiple shots were stacked to enhance the signal-to-noise ratio. For obtaining the passive data, a passive roadside acquisition method is used by taking advantage of moving traffic for producing the low frequency ambient noise. Using passive survey, raw data were obtained at different sampling intervals (2 to 8 ms) and recording times (30 to 120 s) are used to enhance the dispersion curve quality. Corresponding

dispersion curves have been extracted from velocity to frequency diagram. For more detail regarding the passive data recording and parametric study refer to Anbazhagan et al. [36].

The recorded raw data have been further processed to obtain the dispersion curve (DC) and finally to develop the 1D shear wave velocity profile.  $V_s$  profiles of each location were obtained using window-based program named ‘SurfSeis 5’ and ‘ParkSEIS 2’. Both the software use the recorded Rayleigh wave and generate  $V_s$  profiles by analyzing the fundamental mode of dispersion curve of it. To obtain the 1D  $V_s$  profiles, the obtained dispersion curve is inverted using the optimization technique defined in Xia et al. [30]. The quality of data is distinguished based on high SNR of the fundamental-mode dispersion energy. In most of the active surveys, DC was extracted for about 5 to 70 Hz. DC having maximum SNR shows the best fit. For passive data, a number of surveys have been done at the same location by varying the sample interval and time of



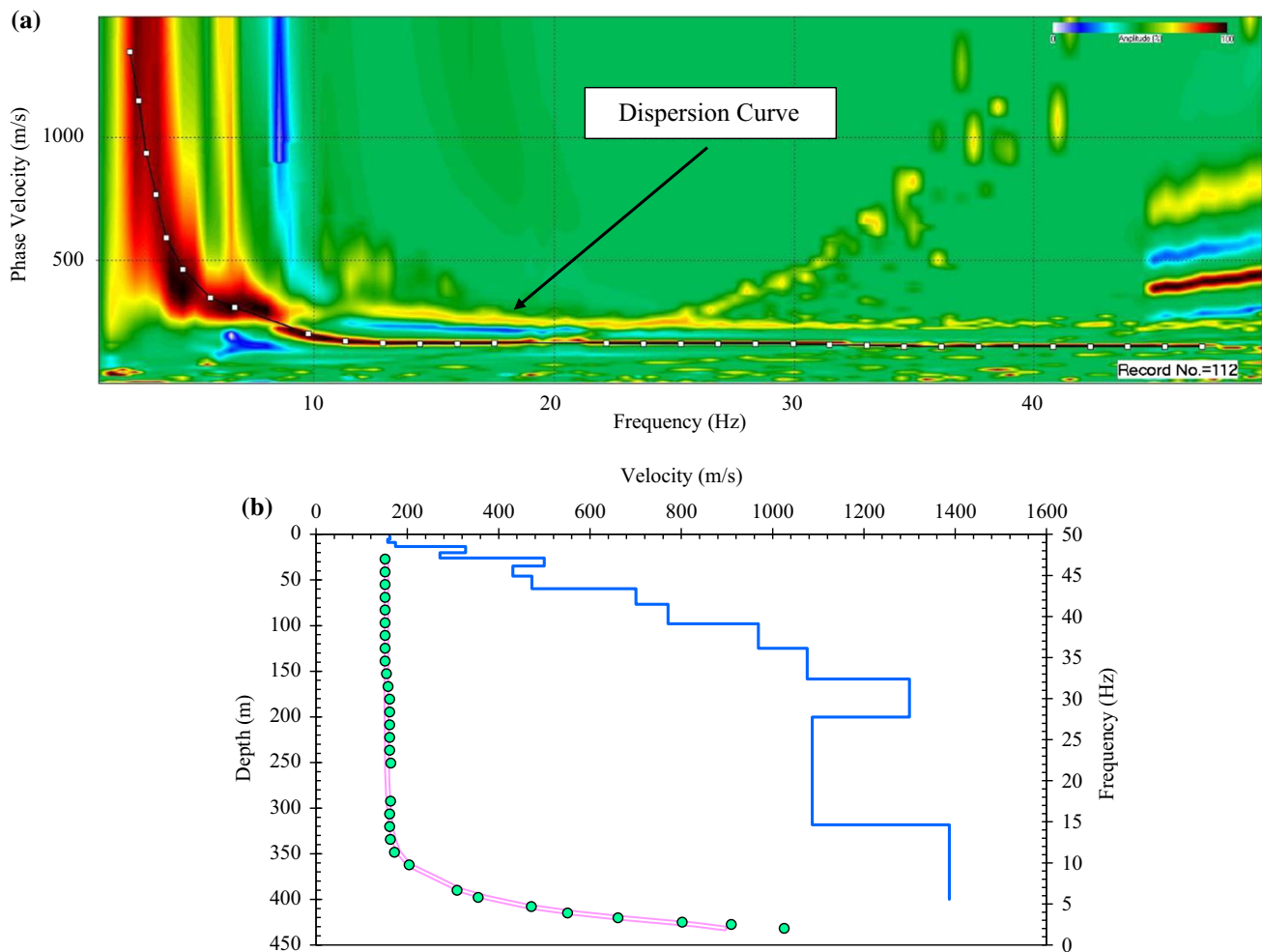


**Fig. 3** Typical **a** dispersion curve and **b**  $V_s$  profile for combined data

recording. Each of the passive recordings is first evaluated independently and then superimposed on each other, afterward smoothed to obtain the DC. DC obtained in the passive survey is having frequency range between 2 and 30 Hz. As discussed above, for most of the data to get the enhanced shear wave velocity at lower frequency, as well as deeper depth, combined DC has been used. The dispersion curve for combined data is given in Fig. 3. Layer model of 15 to 18 is considered at initial stage of inversion [29]. Using the optimization technique [30], 1D  $V_s$  is determined for each iteration. Several iterations are performed to get the minimum smoothing between theoretical and observed DC. Root mean square (RMS) is the best indicator for the closeness between theoretical and observed DC. Several iterations have been performed, while the first 10 iterations showed minimum smoothing between theoretical and observed DC with the RMS error of 1% and a mean velocity variation of 5 m/s. Each DC is individually inverted to get 1D shear wave velocity profile. The match having lower RMS error value (1 to 7%)

between the two curves was chosen as the final 1D shear wave velocity profile of the site. The details about processing and extraction of dispersion curve and  $V_s$  profiles are presented in Bajaj and Anbazhagan [28].

#### Relation Between $V_{SZ}$ and $V_{S30}$ , $z < 30$

Several methods (destructive or nondestructive) are available for estimating the in situ shear wave velocity, but all the methods have certain limitations. For numerous reasons, sometimes it is difficult to obtain shear wave velocity up to a depth of 30 m. In many cases, it is either a technique limitation or environmental-related issues or exceeding predetermined velocity thresholds or budgetary constraints. These also include physical limitations, such as shallow penetration using active source in case of noninvasive method (e.g., spectral analysis of surface waves) or the presence of coarser material while using seismic cone penetrometer. Various researchers [e.g., 6, 7] have proposed different empirical approaches/relations to obtain the

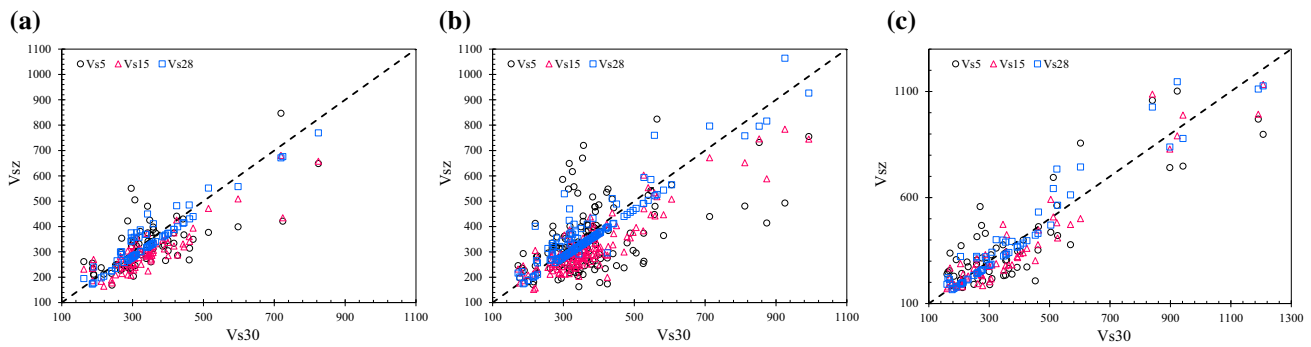


**Fig. 4** Typical comparison of  $V_{S30}$  and  $V_{SZ}$  with  $z$  equal to 5, 15 and 28 m for **a** PHR, **b** UPR and **c** BR

shear velocity at 30 m depth for different regions. These relations are region-specific and may not be directly applicable to another region especially for the IGB, as the soil contains peculiar geological formation and has high silt content. Hence, in this study, relationships between  $V_{SZ}$  and  $V_{S30}$  for a set of  $z$  less than 30 m have been derived.

$V_{SZ}$  is the time-average shear wave velocity to depth  $z$ , computed using the equation

$$V_{SZ} = z/tt(z) \tag{1}$$

where  $tt(z)$  is the shear wave velocity travel time from the surface to depth  $z$ .

The correlation between  $V_{SZ}$  and  $V_{S30}$  has been derived from 275 sites for the Indo-Gangetic Basin by dividing it into three regions, i.e., PHR, UPR and BR. Out of 275 profiles, 75, 130 and 70 profiles are considered for PHR, UPR and BR, respectively. For all the three sites, time average shear wave velocity has been calculated at depths of 5, 6, 7, 8, 9, 10, 11, 12, 13, 14, 15, 16, 17, 18, 19, 20, 21, 22, 23, 24, 25, 26, 27, 28, 29 and 30 m.  $V_{S30}$  varies from 151 to 825 m/s, 162 to 992 m/s, 155 to 1026 m/s in case of

PHR, UPR and BR. As per NEHRP seismic site class, 71%, 54% and 55% data of PHR, UPR and BR sites are of seismic site class D. About 80%, 73%, 70% data have  $V_{S30}$  less than 400 m/s in case of PHR, UPR and BR, respectively. Comparison of  $V_{S30}$  and  $V_{SZ}$  with  $z$  equal to 5, 15 and 28 m is given in Fig. 4a–c for PHR, UPR and BR, respectively. Further, Fig. 5 shows the correlation coefficient between  $V_{S30}$  and  $V_{SZ}$ . The correlation improves as  $V_{SZ}$  is approaching  $V_{S30}$ . However, there is sudden decrease in correlation when depth is increased to 100 m, which will be discussed in the next section.

For obtaining the relationship between  $V_{SZ}$  and  $V_{S30}$ , authors have either used linear [e.g., 6, 8] or nonlinear [7, 9] models. Mostly, linear regression technique is used in obtaining the relationship between  $V_{SZ}$  and  $V_{S30}$ . As suggested by Boore et al. [7], second-order polynomial equation is sufficient to model between  $V_{SZ}$  and  $V_{S30}$ . Hence, in this study, the following equation is used for the fit of the IGB data.

$$\log V_{S30} = b_1 + b_2 \log V_{SZ} + b_3 (\log V_{SZ})^2 \tag{2}$$

**Fig. 5** Correlation between  $V_{S30}$  and  $V_{SZ}$

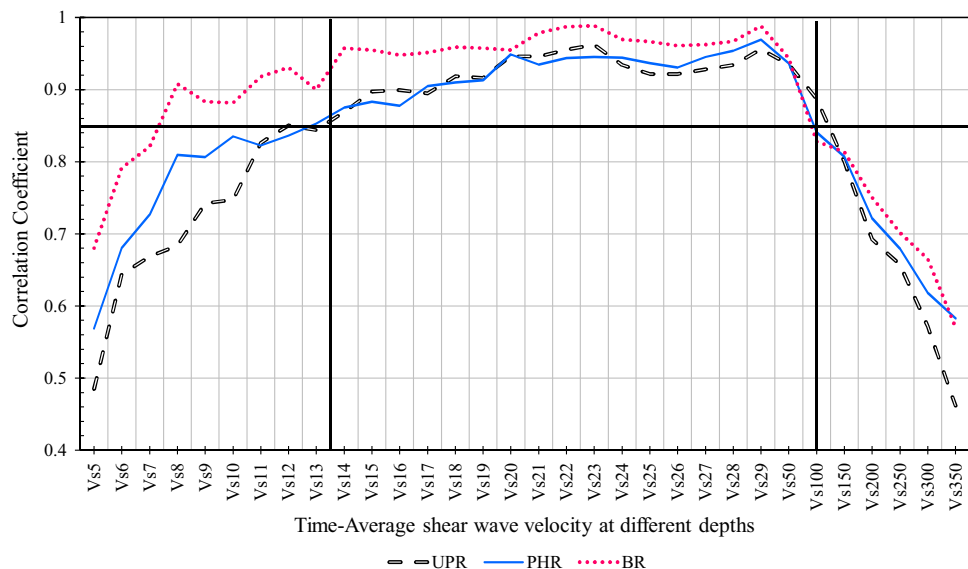


**Table 1** Regression coefficients corresponding to  $V_{S30}$  and  $V_{SZ}$

Y	X	Linear				Ortho			
		$b_1$	$b_2$	$b_3$	Error	$b_1$	$b_2$	$b_3$	Error
<i>(a) For PHR using Eq. 2</i>									
$V_{S30}$	$V_{S5}$	0.391	1.151	- 0.037	0.204	- 1.456	1.475	- 0.037	0.176
$V_{S30}$	$V_{S6}$	11.389	- 2.819	0.325	0.192	- 3.239	2.076	- 0.082	0.159
$V_{S30}$	$V_{S7}$	1.236	0.855	- 0.010	0.212	- 0.665	1.258	- 0.022	0.165
$V_{S30}$	$V_{S8}$	8.030	- 1.500	0.193	0.182	- 5.950	3.067	- 0.177	0.154
$V_{S30}$	$V_{S9}$	3.476	0.054	0.068	0.173	- 4.973	2.884	- 0.167	0.141
$V_{S30}$	$V_{S10}$	1.516	0.599	0.027	0.162	- 6.997	3.346	- 0.193	0.137
$V_{S30}$	$V_{S11}$	0.650	0.922	- 0.004	0.157	- 12.946	5.338	- 0.359	0.139
$V_{S30}$	$V_{S12}$	4.420	- 0.354	0.104	0.162	- 4.612	2.535	- 0.125	0.135
$V_{S30}$	$V_{S13}$	- 4.229	2.591	- 0.146	0.149	- 6.660	3.302	- 0.196	0.120
$V_{S30}$	$V_{S14}$	- 4.789	2.732	- 0.154	0.133	- 14.130	5.759	- 0.397	0.103
$V_{S30}$	$V_{S15}$	6.933	- 1.323	0.198	0.136	- 6.159	3.029	- 0.162	0.113
$V_{S30}$	$V_{S16}$	4.888	- 0.581	0.130	0.142	- 1.672	1.505	- 0.034	0.116
$V_{S30}$	$V_{S17}$	0.009	1.071	- 0.010	0.125	- 3.687	2.222	- 0.099	0.101
$V_{S30}$	$V_{S18}$	- 6.720	3.327	- 0.199	0.111	- 9.899	4.320	- 0.275	0.087
$V_{S30}$	$V_{S19}$	- 5.879	3.062	- 0.179	0.116	- 9.727	4.281	- 0.274	0.090
$V_{S30}$	$V_{S20}$	2.407	0.230	0.064	0.106	- 3.079	2.046	- 0.085	0.082
$V_{S30}$	$V_{S21}$	1.787	0.420	0.049	0.109	- 3.081	2.001	- 0.079	0.084
$V_{S30}$	$V_{S22}$	2.701	0.132	0.071	0.107	- 1.514	1.511	- 0.041	0.083
$V_{S30}$	$V_{S23}$	- 0.169	1.124	- 0.015	0.101	- 2.186	1.757	- 0.064	0.075
$V_{S30}$	$V_{S24}$	- 0.868	1.368	- 0.037	0.103	- 3.672	2.263	- 0.107	0.076
$V_{S30}$	$V_{S25}$	0.951	0.785	0.010	0.119	- 3.063	2.076	- 0.093	0.088
$V_{S30}$	$V_{S26}$	0.572	0.945	- 0.007	0.126	- 2.424	1.891	- 0.081	0.093
$V_{S30}$	$V_{S27}$	3.973	- 0.314	0.109	0.108	2.089	0.267	0.065	0.083
$V_{S30}$	$V_{S28}$	3.503	- 0.154	0.095	0.099	2.477	0.145	0.074	0.075
$V_{S30}$	$V_{S29}$	2.474	0.180	0.067	0.083	1.873	0.347	0.056	0.063
<i>(b) For UPR using Eq. 2</i>									
$V_{S30}$	$V_{S5}$	7.887	- 1.119	0.133	0.304	11.554	- 2.570	0.273	0.279
$V_{S30}$	$V_{S6}$	17.381	- 4.792	0.488	0.354	10.817	- 2.641	0.314	0.202
$V_{S30}$	$V_{S7}$	11.125	- 2.498	0.276	0.223	7.877	- 1.566	0.212	0.200
$V_{S30}$	$V_{S8}$	12.217	- 2.912	0.314	0.210	8.566	- 1.851	0.240	0.187
$V_{S30}$	$V_{S9}$	9.190	- 1.900	0.236	0.218	5.954	- 0.899	0.161	0.194
$V_{S30}$	$V_{S10}$	8.031	- 1.489	0.193	0.202	6.650	- 1.194	0.184	0.180
$V_{S30}$	$V_{S11}$	11.984	- 2.995	0.336	0.165	3.604	- 0.249	0.113	0.143
$V_{S30}$	$V_{S12}$	7.881	- 1.540	0.207	0.170	2.784	0.100	0.077	0.145
$V_{S30}$	$V_{S13}$	7.571	- 1.415	0.194	0.174	2.864	0.092	0.075	0.149
$V_{S30}$	$V_{S14}$	9.175	- 2.010	0.249	0.158	1.638	0.464	0.047	0.136
$V_{S30}$	$V_{S15}$	7.492	- 1.408	0.196	0.155	1.051	0.704	0.024	0.129
$V_{S30}$	$V_{S16}$	7.834	- 1.529	0.206	0.153	0.854	0.743	0.022	0.130
$V_{S30}$	$V_{S17}$	2.996	0.092	0.070	0.147	- 1.097	1.381	- 0.030	0.124
$V_{S30}$	$V_{S18}$	4.899	- 0.585	0.130	0.137	1.602	0.462	0.047	0.112
$V_{S30}$	$V_{S19}$	2.823	0.128	0.069	0.137	- 0.202	1.092	- 0.007	0.111
$V_{S30}$	$V_{S20}$	- 1.274	1.505	- 0.046	0.111	- 3.420	2.184	- 0.099	0.088
$V_{S30}$	$V_{S21}$	- 1.392	1.525	- 0.047	0.112	- 3.608	2.221	- 0.101	0.089
$V_{S30}$	$V_{S22}$	- 0.998	1.403	- 0.038	0.104	- 1.692	1.600	- 0.051	0.082
$V_{S30}$	$V_{S23}$	1.420	0.540	0.038	0.099	0.771	0.724	0.025	0.078
$V_{S30}$	$V_{S24}$	0.200	0.971	0.000	0.118	- 1.022	1.343	- 0.027	0.095

**Table 1** continued

Y	X	Linear				Ortho			
		$b_1$	$b_2$	$b_3$	Error	$b_1$	$b_2$	$b_3$	Error
$V_{S30}$	$V_{S25}$	1.602	0.556	0.030	0.137	− 0.424	1.176	− 0.016	0.110
$V_{S30}$	$V_{S26}$	0.807	0.822	0.008	0.137	− 0.938	1.342	− 0.030	0.111
$V_{S30}$	$V_{S27}$	− 0.699	1.310	− 0.032	0.128	− 1.261	1.439	− 0.038	0.104
$V_{S30}$	$V_{S28}$	− 0.206	1.137	− 0.017	0.124	− 0.140	1.062	− 0.007	0.100
$V_{S30}$	$V_{S29}$	− 0.477	1.208	− 0.022	0.102	− 0.183	1.077	− 0.008	0.085
<i>(c) for BR using Eq. 2</i>									
$V_{S30}$	$V_{S5}$	9.652	− 2.009	0.230	0.248	− 2.246	1.769	− 0.066	0.238
$V_{S30}$	$V_{S6}$	5.836	− 0.896	0.160	0.208	− 11.193	4.825	− 0.315	0.178
$V_{S30}$	$V_{S7}$	6.051	− 0.769	0.125	0.305	− 2.801	2.016	− 0.091	0.228
$V_{S30}$	$V_{S8}$	4.269	− 0.309	0.099	0.232	− 3.783	2.251	− 0.102	0.185
$V_{S30}$	$V_{S9}$	3.529	0.014	0.072	0.251	− 3.762	2.429	− 0.125	0.196
$V_{S30}$	$V_{S10}$	− 0.274	1.280	− 0.039	0.254	− 5.362	2.862	− 0.159	0.191
$V_{S30}$	$V_{S11}$	− 3.131	2.074	− 0.090	0.175	− 10.306	4.363	− 0.270	0.135
$V_{S30}$	$V_{S12}$	0.962	0.728	0.019	0.184	− 7.413	3.427	− 0.196	0.144
$V_{S30}$	$V_{S13}$	1.511	0.585	0.027	0.213	− 3.688	2.225	− 0.100	0.160
$V_{S30}$	$V_{S14}$	0.784	0.773	0.018	0.159	− 2.926	1.962	− 0.076	0.120
$V_{S30}$	$V_{S15}$	− 0.591	1.265	− 0.026	0.168	− 0.591	1.265	− 0.026	0.128
$V_{S30}$	$V_{S16}$	0.610	0.873	0.004	0.180	− 4.148	2.385	− 0.114	0.136
$V_{S30}$	$V_{S17}$	− 0.430	1.170	− 0.016	0.156	− 3.972	2.294	− 0.104	0.117
$V_{S30}$	$V_{S18}$	0.105	0.977	0.003	0.139	− 2.587	1.841	− 0.065	0.103
$V_{S30}$	$V_{S19}$	0.769	0.756	0.020	0.147	− 3.044	1.984	− 0.078	0.110
$V_{S30}$	$V_{S20}$	− 0.886	1.363	− 0.034	0.151	− 4.293	2.452	− 0.120	0.112
$V_{S30}$	$V_{S21}$	0.906	0.717	0.023	0.127	− 2.053	1.676	− 0.054	0.096
$V_{S30}$	$V_{S22}$	1.147	0.656	0.026	0.120	− 1.865	1.641	− 0.053	0.088
$V_{S30}$	$V_{S23}$	0.422	0.906	0.005	0.109	− 1.278	1.455	− 0.039	0.079
$V_{S30}$	$V_{S24}$	2.537	0.173	0.067	0.125	0.778	0.737	0.023	0.089
$V_{S30}$	$V_{S25}$	1.906	0.395	0.047	0.139	− 0.388	1.126	− 0.010	0.100
$V_{S30}$	$V_{S26}$	3.850	− 0.243	0.099	0.151	1.419	0.533	0.038	0.107
$V_{S30}$	$V_{S27}$	2.782	0.143	0.064	0.146	1.545	0.526	0.035	0.102
$V_{S30}$	$V_{S28}$	1.620	0.515	0.035	0.137	0.257	0.939	0.002	0.097
$V_{S30}$	$V_{S29}$	1.562	0.489	0.041	0.099	0.482	0.833	0.014	0.070

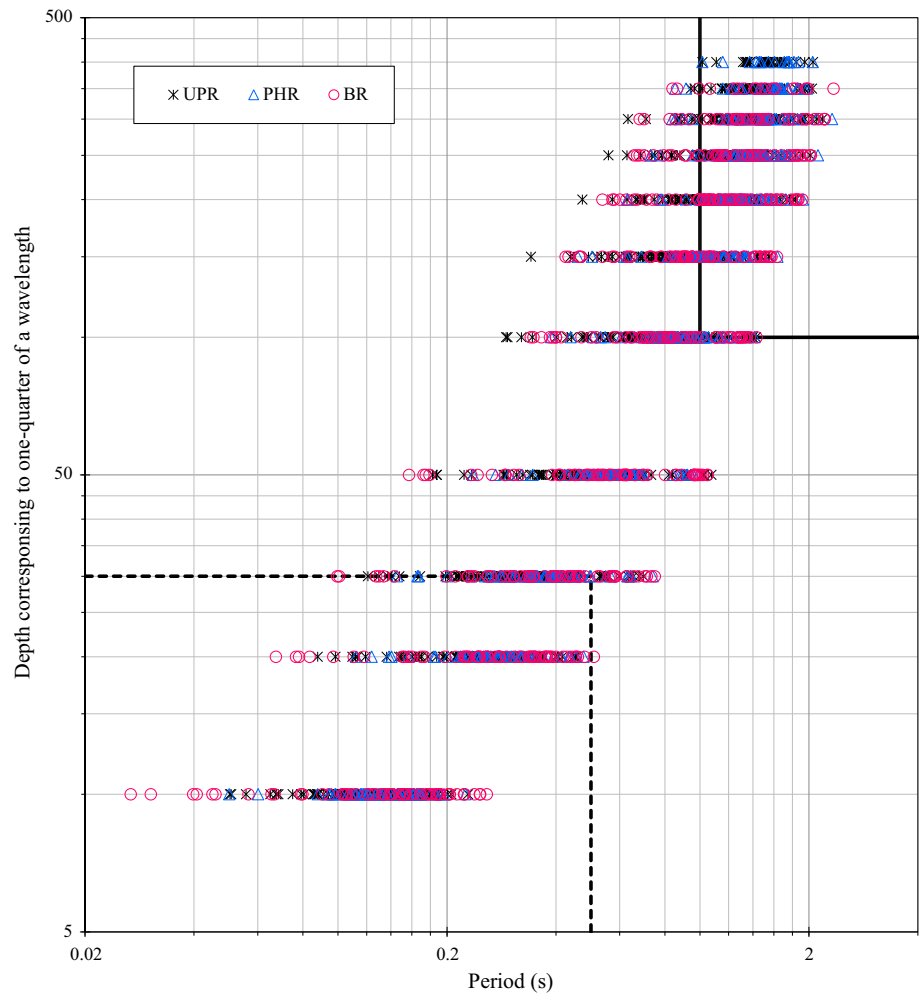
Here,  $b_1$ ,  $b_2$  and  $b_3$  are the regression coefficients. In this study, both orthogonal linear and nonlinear regression and least square approach are used in deriving the relationship between  $V_{SZ}$  and  $V_{S30}$  (See Eq. 2). Further, standard deviation from all the approaches has been compared. The derived regression coefficients corresponding to least square approach and orthogonal approach are given in Table 1a–c for PHR, UPR and BR. In addition to the regression coefficients, error in the equations is estimated. It is equivalent to the standard deviation in the predicted equations. The lower the deviation, the better the regression equation. Overall error in case of orthogonal is less as compared to least square approach (See Table 1).

**Relation Between  $V_{SZ}$  and  $V_{S30}$ ,  $z > 30$**

There is an ongoing debate on considering time-average shear wave velocity up to 30 m depth, i.e.,  $V_{S30}$  as an effective parameter for site amplification. Few researchers [e.g., 37] commented that considering  $V_s$  up to 30 m depth is too shallow to reflect the velocity structure as that can affect periods that are more extended than a few tenths of a second (2011). Figure 6 shows the depth corresponding to one-quarter of wavelength for various periods for deep profiles of IGB. For each of the profile, period is computed using Eq. 3.

$$T = 4z/V_{SZ} \tag{3}$$

**Fig. 6** Comparison of depth corresponding to one-quarter of a wavelength with period for the IGB. Each symbol represents the velocity profile at an individual site. At each of the points,  $V_{SZ}$  has been determined with  $z$  varying as 10, 20, 30, 50, 100, 150, 200, 250, 300, 350 and 400 m. Further using the  $z$  value and corresponding  $V_{SZ}$ ,  $T$  has been calculated using Eq. 3



where  $z = z_{\max}$  is used to compute the period  $T$  for which  $z_{\max}$  is one-quarter of a wavelength. Figure 6 shows the depth that equals one-quarter of a wavelength with a velocity equal to the time-averaged velocity between the varying depth (10, 20, 30, 50, 100, 150, 200, 250, 300, 350 and 400 m) of different profiles and the surface. Each symbol in Fig. 6 represents a velocity profile. At each of the points,  $V_{SZ}$  has been determined with  $z$  varying as 10, 20, 30, 50, 100, 150, 200, 250, 300, 350 and 400 m. Further, using the  $z$  value and corresponding  $V_{SZ}$ ,  $T$  has been calculated using Eq. 3. For each site, period has been estimated for the depth corresponding to one-quarter of wavelength, if site amplification is controlled by velocities within one-quarter wavelength of the surface [e.g., 38–40]. Figure 6 can also be used to estimate the minimum depth required to provide site amplification information for a given period for IGB. It can also be interpreted from Fig. 6 that, for estimating the amplifications at periods as long as 1 s, the profile must extend to at least 100 m in case of IGB. It can be also noted here that Boore et al. [7] has concluded that, to estimate amplifications at periods as

long as 2 s, at least 100 m velocity profile is needed to be considered. Similar to Boore et al. [7], velocities known up to 30 m depth are relevant for site amplification at a period less than 1 s, more specifically up to 0.5 s (See Fig. 6). Hence, in this study, further,  $V_{S30}$  is correlated with  $V_{SZ}$ , with  $z$  equals to 50, 100, 150, 200, 250, 300 and 350 m.

Figure 5 shows that correlation between  $V_{S30}$  and  $V_{SZ}$  is decreasing drastically for depth greater than 100 m. However, Boore et al. [7] showed that for Japan data,  $V_{S30}$  and  $V_{SZ}$  hold a good correlation till 200 m. Undoubtedly, the variability between  $V_{S30}$  and  $V_{SZ}$  increases with depth. However, it becomes constant after a particular depth, say after 200 m, as the correlation is almost constant for all the three regions (See Fig. 5). For finding the relation between  $V_{S30}$  and  $V_{SZ}$ , for  $z$  more than 30 m, both least square and orthogonal approaches are used. The following equation is used to find the relation between  $V_{S30}$  and  $V_{SZ}$

$$\log V_{30} = b_1 + b_2 \log V_{SZ} \tag{4}$$

Here,  $b_1$  and  $b_2$  are the regression coefficients and  $V_{SZ}$  represents the time average shear wave velocity at 50, 100,

**Table 2** Regression coefficients corresponding to  $V_{S30}$  and  $V_{SZ}$  for  $z$  more than 30 m

Y	X	Linear			Ortho				
		$b_1$	$b_2$	Error	$b_1$	$b_2$	Error		
<i>(a) For PHR, UP, and BR using Eq. 4</i>									
<b>UPR</b>									
$V_{S30}$	$V_{S50}$	0.203	0.951	0.120	- 0.102	1.002	0.092		
$V_{S30}$	$V_{S100}$	- 0.419	1.004	0.158	- 1.086	1.111	0.121		
$V_{S30}$	$V_{S150}$	- 0.584	0.995	0.193	- 1.637	1.157	0.149		
$V_{S30}$	$V_{S200}$	- 0.712	0.999	0.225	- 2.370	1.251	0.172		
$V_{S30}$	$V_{S250}$	- 1.536	1.102	0.224	- 3.621	1.413	0.169		
$V_{S30}$	$V_{S300}$	- 1.944	1.150	0.227	- 4.404	1.511	0.165		
$V_{S30}$	$V_{S350}$	- 1.393	1.049	0.213	- 5.955	1.714	0.144		
<b>PHR</b>									
$V_{S30}$	$V_{S50}$	- 0.129	1.009	0.116	- 0.693	1.105	0.081		
$V_{S30}$	$V_{S100}$	- 0.770	1.068	0.170	- 2.194	1.301	0.122		
$V_{S30}$	$V_{S150}$	- 0.585	0.999	0.192	- 2.324	1.273	0.142		
$V_{S30}$	$V_{S200}$	- 1.421	1.113	0.196	- 3.326	1.408	0.140		
$V_{S30}$	$V_{S250}$	- 1.534	1.109	0.206	- 3.726	1.443	0.143		
$V_{S30}$	$V_{S300}$	- 2.210	1.196	0.200	- 4.796	1.583	0.127		
<b>BR</b>									
$V_{S30}$	$V_{S50}$	0.140	0.959	0.139	- 0.090	0.997	0.100		
$V_{S30}$	$V_{S100}$	- 1.260	1.137	0.196	- 2.010	1.257	0.127		
$V_{S30}$	$V_{S150}$	- 2.053	1.219	0.237	- 3.202	1.395	0.147		
$V_{S30}$	$V_{S200}$	- 2.572	1.280	0.251	- 4.367	1.552	0.150		
$V_{S30}$	$V_{S250}$	- 2.290	1.212	0.263	- 4.538	1.546	0.157		
$V_{S30}$	$V_{S300}$	- 2.995	1.303	0.250	- 5.287	1.642	0.142		
Y	X	Linear				Ortho			
		$b_1$	$b_2$	$b_3$	Error	$b_1$	$b_2$	$b_3$	Error
<i>(b) for PHR, UP, and BR for second degree polynomial equation (Eq. 2)</i>									
<b>UPR</b>									
$V_{S30}$	$V_{S50}$	- 0.454	1.168	- 0.018	0.120	- 1.219	1.371	- 0.030	0.093
$V_{S30}$	$V_{S100}$	- 2.628	1.697	- 0.054	0.159	- 4.177	2.082	- 0.076	0.122
$V_{S30}$	$V_{S150}$	- 3.389	1.846	- 0.065	0.193	- 1.895	1.236	- 0.006	0.150
$V_{S30}$	$V_{S200}$	- 9.505	3.638	- 0.198	0.225	3.124	- 0.407	0.125	0.172
$V_{S30}$	$V_{S250}$	- 7.695	2.913	- 0.133	0.225	2.727	- 0.470	0.140	0.169
$V_{S30}$	$V_{S300}$	- 0.228	0.649	0.037	0.228	11.899	- 3.263	0.349	0.165
$V_{S30}$	$V_{S350}$	- 5.594	2.267	- 0.088	0.215	- 9.562	2.761	- 0.076	0.145
<b>PHR</b>									
$V_{S30}$	$V_{S50}$	3.427	- 0.194	0.101	0.116	0.356	0.751	0.030	0.081
$V_{S30}$	$V_{S100}$	- 2.054	1.480	- 0.033	0.171	- 10.275	3.897	- 0.208	0.122
$V_{S30}$	$V_{S150}$	2.094	0.173	0.063	0.193	- 16.425	5.623	- 0.335	0.141
$V_{S30}$	$V_{S200}$	5.752	- 1.072	0.166	0.197	- 16.219	5.337	- 0.299	0.140
$V_{S30}$	$V_{S250}$	12.156	- 2.984	0.306	0.206	- 19.385	6.128	- 0.350	0.143
$V_{S30}$	$V_{S300}$	22.824	- 6.188	0.544	0.198	- 20.620	6.236	- 0.342	0.127
<b>BR</b>									
$V_{S30}$	$V_{S50}$	3.294	- 0.084	0.086	0.140	1.364	0.518	0.039	0.100
$V_{S30}$	$V_{S100}$	5.455	- 0.998	0.169	0.197	8.792	- 2.171	0.271	0.124
$V_{S30}$	$V_{S150}$	1.344	0.176	0.080	0.235	15.762	- 4.446	0.449	0.152
$V_{S30}$	$V_{S200}$	9.334	- 2.318	0.271	0.251	14.257	- 4.066	0.423	0.148
$V_{S30}$	$V_{S250}$	- 1.001	0.829	0.028	0.266	19.296	- 5.538	0.525	0.154
$V_{S30}$	$V_{S300}$	0.075	0.402	0.066	0.254	25.300	- 7.337	0.658	0.138

150, 200, 250, 300 and 350 m. For all the three regions,  $b_1$  and  $b_2$  are determined using both least square and orthogonal approaches using Eq. 4. The derived regression coefficients corresponding to least square approach and orthogonal approach are given in Table 2a for PHR, UPR and BR. Similar to Boore et al. [7], second-order polynomial equation (See Eq. 1) is also used for deriving the equation between  $V_{S30}$  and  $V_{SZ}$  for  $z$  more than 30 m. Coefficients corresponding to least square and orthogonal regression are given in Table 2b. Further, residual analysis has been used for determining the best suitable functional form for correlating  $V_{S30}$  and  $V_{SZ}$  for  $z$  more than 30 m. Typical example of residual analysis of UPR is given in Fig. 7. Figure 7a and b shows the residual variation between  $V_{S30}$  and  $V_{S50}$  and  $V_{S30}$  and  $V_{S250}$ , respectively. Further, the average value up to 200, 250, 300, 350, 400, 500, 600 and 1000 m/s has been calculated to determine the best suitable equation for correlating  $V_{S30}$  and  $V_{SZ}$  for  $z$  more than 30 m. Based on the analysis, it can be concluded that, orthogonal linear equation is predicting better till  $V_{S30} \leq 300$  m/s (Eq. 4) and for  $V_{S30} > 300$  m/s (Eq. 1) orthogonal nonlinear equation is predicting better. It can be recommended that for correlating  $V_{S30}$  and  $V_{SZ}$  for either  $z$  more than or less than 30 m depth, orthogonal regression analysis can be used for better  $V_{S30}$  prediction.

**Relationship Between  $V_{S30}$  and  $N_z$ ,  $5 < z < 50$**

The study area has been classified as per NEHRP [41], and the distribution of  $V_{S30}$  is given in Fig. 8. Kriging interpolation method has been used in developing the spatial variation map of  $V_{S30}$ . Lambert conformal conic has been used as map projection system, and Geodetic datum has been used as datum reference frame. The map scaling has been done as per the Indian Grid system (

<https://deepradhan.heliohost.org/gis/indian-grid/>, last accessed May 2019). The blue lines in Fig. 8 are representing Rivers. Even though  $V_S$  values predominately considered for amplification related studies in most of modern codes, Indian seismic code 1893–2016 (BIS:1893, 40) classifies sites considering average Standard Penetration Test (SPT)  $N$  values up to 30 m ( $N_{30}$ ). The recent version of BIS:1893 [20] has given the design acceleration response spectra which is dependent on weighted average uncorrected  $N$  value till 30 m depth ( $N_{30}$ ). The three-soil classification is given in BIS:1893 [20]. These classifications are

- Type A—Rock or Hard soil and  $N_{30}$  value above 30
- Type B—Medium or stiff soil and  $N_{30}$  between 10 and 30
- Type C—Soft soil and  $N_{30}$  less than 10

Developing  $N_{30}$  map of the IGB requires extensive drilling and costly procedure. Hence, in this study, an attempt has been made to develop a relationship between  $V_{S30}$  and  $N_z$ ,  $z$  equals to 5, 10, 20, 30, 40 and 50 m using available SPT bore logs in IGB. Since only 52 bore log data with SPT-N value are available,  $V_{S30}$  and  $N_z$  relationship for the whole IGB has been developed instead of separating that into three regions. For finding the relation between  $V_{S30}$  and  $N_z$ , for  $5 < z < 50$ , both least square and orthogonal approaches are used. The following equation is used to find the relation between  $V_{S30}$  and  $V_{SZ}$

$$V_{S30} = c_1 N_z^{c_2}, \quad 5 < z < 50 \tag{5}$$

Based on the analysis, it is observed that power law has more coefficient of determination value as compared to linear regression; hence, power law is used in determining the regression coefficients. The derived regression coefficients corresponding to least square approach and

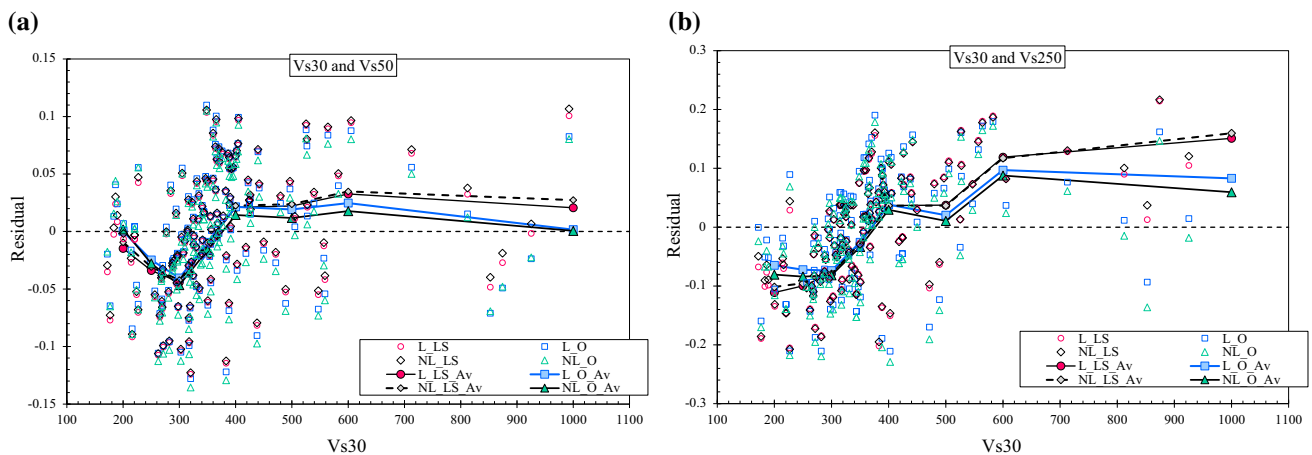


**Fig. 7** Typical residual variation of correlation between  $V_{S30}$  and **a**  $V_{S50}$ , and **b**  $V_{S250}$  for UPR. L\_LS, L\_O, NL\_LS and NL\_O represent the regression coefficients determined using least square linear,

orthogonal linear, least square nonlinear and orthogonal nonlinear equations respectively. L\_LS\_Av, L\_O\_Av, NL\_LS\_Av and NL\_O\_Av represent the corresponding average values up to different  $V_{S30}$  points

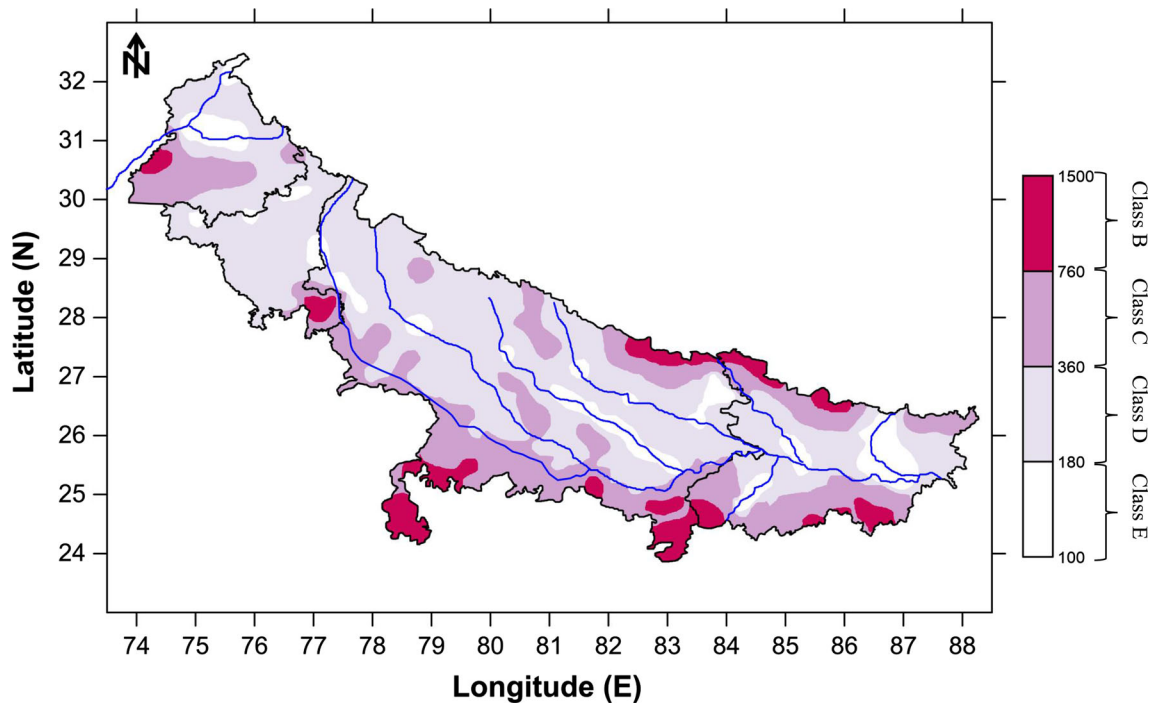


**Fig. 8** Spatial variation of shear wave average up to 30 m depth ( $V_{S30}$ ) for IGB. Class E, Class D, Class C, and Class B are the seismic classification given in NEHPR [41]. The blue lines are representing Rivers (color figure online)

**Table 3** Regression coefficients corresponding to  $V_{S30}$  and  $N_z$ , for  $5 < z < 50$  using Eq. 5

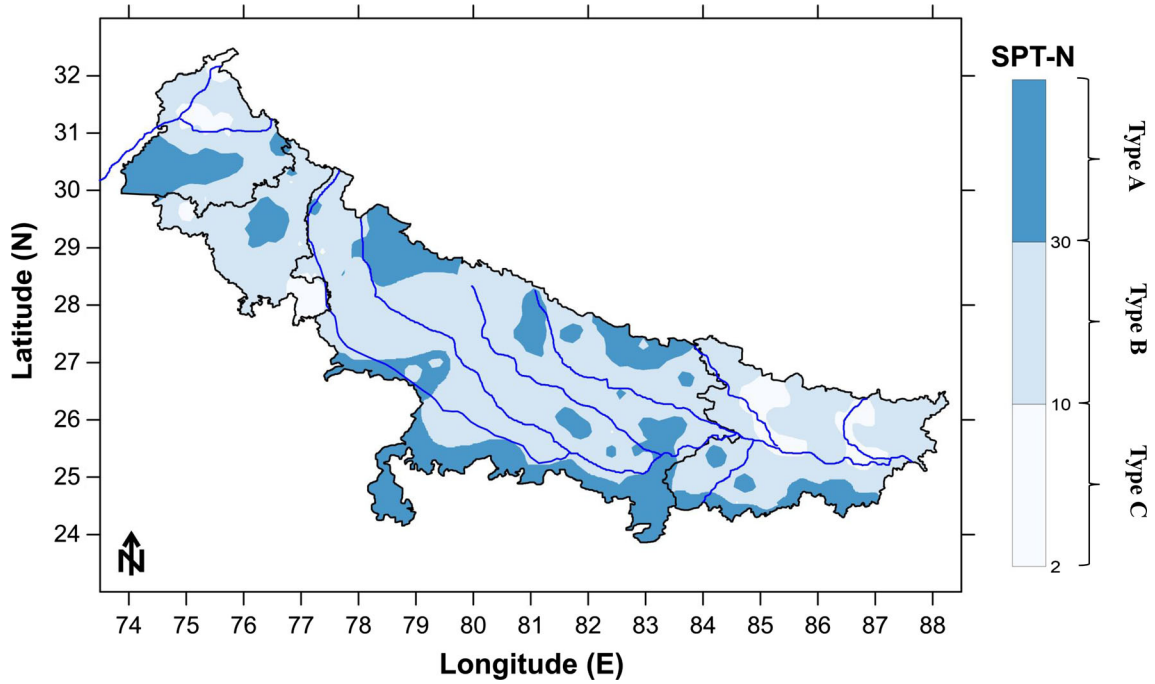
Y	X	Linear			Ortho		
		$c_1$	$c_2$	Error	$c_1$	$c_2$	Error
$V_{S30}$	$N_5$	130.87	0.325	1.678	97.46	0.421	1.354
$V_{S30}$	$N_{10}$	117.68	0.353	1.662	64.07	0.558	1.287
$V_{S30}$	$N_{20}$	102.35	0.384	1.641	50.32	0.619	1.197
$V_{S30}$	$N_{30}$	75.41	0.455	1.504	48.61	0.593	1.005
$V_{S30}$	$N_{40}$	79.85	0.435	1.463	51.45	0.563	0.676
$V_{S30}$	$N_{50}$	86.27	0.407	1.487	51.05	0.556	0.746

orthogonal approach are given in Table 3. It can be seen from Table 3 that error in the case of orthogonal regression is less as compared to least square analysis. The empirical equations derived in this study between  $V_{S30}$  and  $N_{30}$  are further used to map  $V_{S30}$  based on  $N_{30}$ . The distribution of  $V_{S30}$  based on  $N_{30}$  for the IGB is given in Fig. 9. Similar to Fig. 8, Kriging interpolation method, Lambert conformal conic and Geodetic datum have been used in preparation of maps in Figs. 9 and 10. It can be seen from Fig. 9 that most of the IGB is classified as Type B. Few places near to Kosi, Gandhak, Sutluj and New-Delhi are classified as Type C, and the southernmost part of UPR and BR is mostly classified as Type A. In most of the site response study in India, amplification parameters are described based on  $V_{S30}$  instead of  $N_{30}$ . In this study,  $V_{S30}$  (Fig. 8) as per international standards and  $N_{30}$  (Fig. 9) based on  $V_{S30}$

map have been generated using same data. It can be seen that for the regions corresponding to site class E and D, for most of the sites,  $N$  value of more than 15 is observed. However, spatial variation of  $N_{30}$  can be studied in more details for the better implication of BIS:1893 [20] in determination of acceleration response spectra.

Even though SPT-N value is widely used in various geotechnical applications, various factors and corrections are involved in it. These factors include drilling methods, borehole size and stability, blow count rate, hammer configuration, energy corrections, fine contents, etc. The effect of all these factors can be accounted by applying correction factors separately or jointly [42]. However, the corrected SPT-N value does not assure an efficient engineering design unless the true energy losses occurring in the SPT system are considered [43]. Recently, Anbazhagan et al.

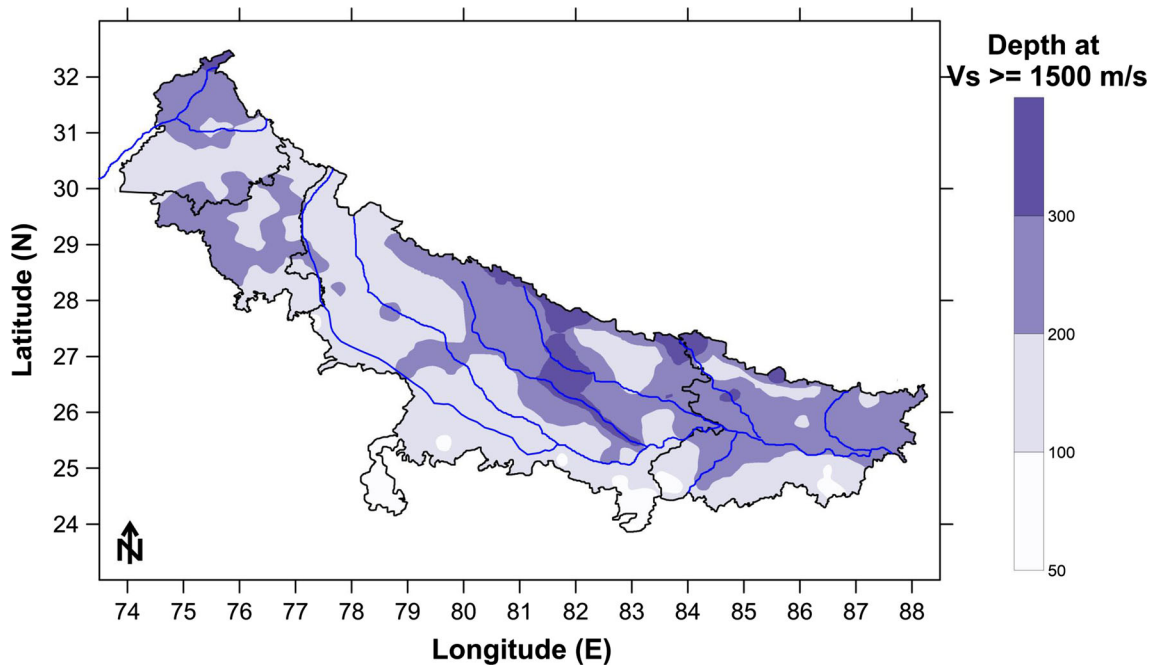




**Fig. 9** Spatial variation of SPT-N average up to 30 m depth ( $N_{30}$ ) for IGB. Type A, Type B and Type C are the seismic classification given in IS-1893 [20]. The blue lines are representing Rivers (color figure online)

[44] also commented on the energy correction factor used for SPT-N value in liquefaction assessment. Hammer energy correction used for SPT-N value may change soil layer category from liquefiable to non-liquefiable in the same borehole [44]. One has to be careful about using uncorrected SPT-N value for accounting site classification

and amplification [46]. It can be also noted here that recently Bajaj and Anbazhagan [45] concluded that input ground motions needs to be given at the layer having  $V_s \geq 1500 \pm 150$  m/s for reliable estimation of site amplification factors at deep soil sites. Hence, the depth distribution of  $V_s$  equal to or more than 1500 m/s is given in



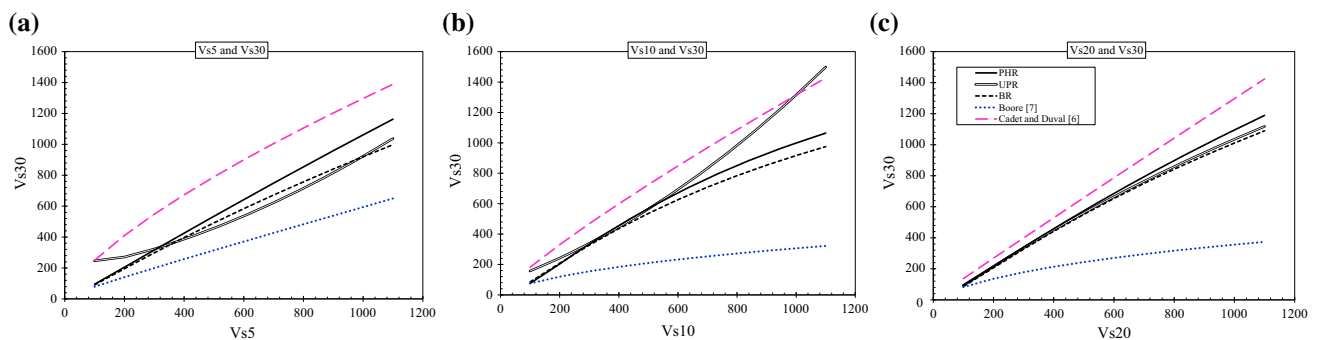
**Fig. 10** Spatial variation of depth at which  $V_s$  is equal to and more than 1500 m/s. The blue lines are representing Rivers (color figure online)

Fig. 10, which can be further used for the preliminary knowledge of depth of investigation required for site specific response study.

### Comparison with Existing Studies

Various correlations have been derived for correlating  $V_{S30}$  and  $V_{SZ}$ . Cadet and Duval [6] developed a linear correlation between  $V_{S30}$  and  $V_{SZ}$ , where  $z$  is equal to 5, 10, 20, 30, 50 and 100 m using KiK-Net data. Boore et al. [7] developed a correlation between  $V_{S30}$  and  $V_{SZ}$  for  $z$  more than and less than 30 m. The velocity profiles used in this study are from Japan, California, Turkey and Europe. The newly developed regression relation between  $V_{S30}$  and  $V_{SZ}$  is compared with Boore et al. [7] and Cadet and Duval [6]. A typical comparison of variation of  $V_{S30}$  and  $V_{SZ}$ , where  $z$  is equal to 5, 10 and 20 m is given in Fig. 11. It can be seen

from Fig. 11 that at lower depths, a significant difference is observed in all the equations. However, Boore et al. [7] are predicting low  $V_{S30}$  values as compared to the equations proposed in the present study. Residuals calculated from Boore et al. [7], Cadet and Duval [6] and present equation have been compared and given as Fig. 12. Figure 12a and b corresponds to the residual variation between  $V_{S30}$  and  $V_{S5}$  and  $V_{S30}$  and  $V_{S20}$  for UPR, PHR, and BR. Based on the residual analysis, it has seen that Boore et al. [7] and Cadet and Duval [6] were not in argument with the Indo-Gangetic Basin deposits for shallow sites. For example, for  $V_{S10}$  equal to 200 m/s, the  $V_{S30}$  for UPR, PHR, BR, Boore et al. [7] and Cadet and Duval [6] regression are 238, 204, 208, 331 and 262 m/s, respectively. Additionally, a typical comparison of observed and calculated  $V_{S30}$  is also given in Table 4. It can be observed from Table 4 that Boore et al. [7] equations are underestimating the  $V_{S30}$  values as



**Fig. 11** Typical comparison of variation of  $V_{S30}$  and  $V_{SZ}$ , where  $z$  is equal to 5, 10 and 20 m considering new equation for three regions and Boore et al. [7] and Cadet and Duval [6]

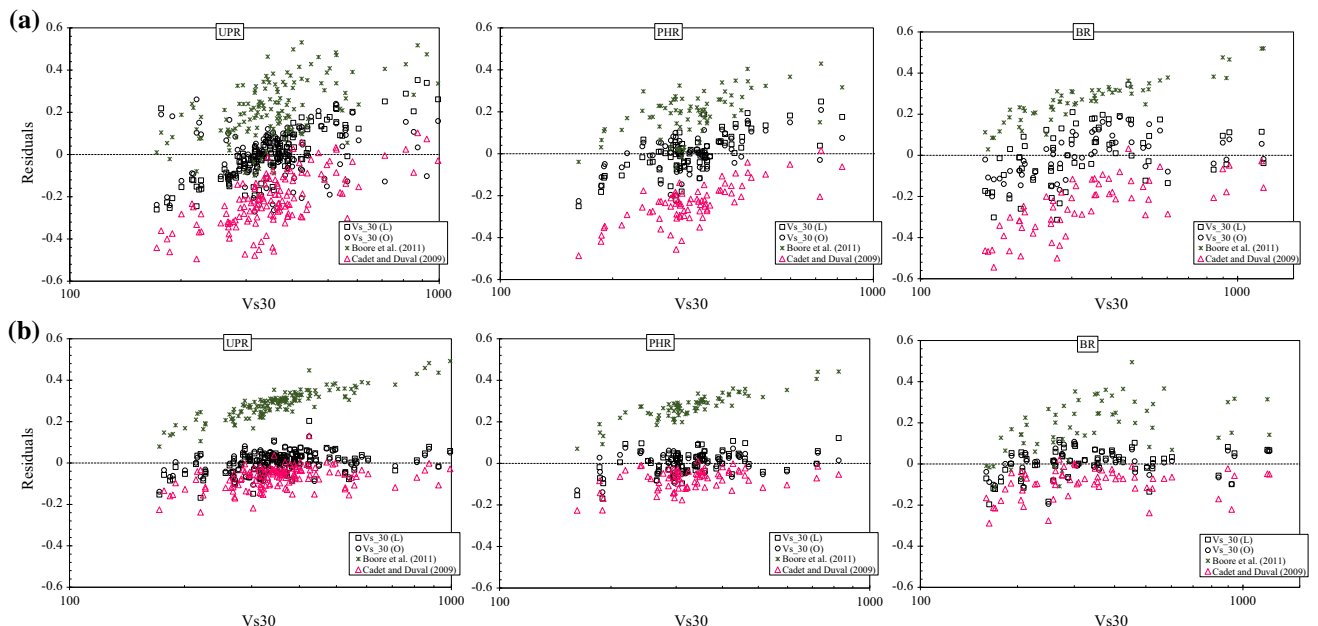


**Fig. 12** Typical comparison of residual from **a**  $V_{S30}$  and  $V_{S5}$  and **b**  $V_{S30}$  and  $V_{S20}$  for PHR, UPR and BR

**Table 4** Typical comparison of observed  $V_{S30}$  with the calculated  $V_{S30}$  using different regression coefficients

	UPR	PHR	BR
Observed $V_{S30}$ (m/s)	320.0315	828.3983	461.5309
Site Class as per NEHRP [4]	D	B	C
Soil deposition	Alluvium	Alluvium	Alluvium
<i>Calculated using the regression equations</i>			
Calculated from the present study using $V_{S5}$ (m/s) considering Eq. 2	332.9087	800.3183	437.597
Calculated from the present study using $V_{S15}$ (m/s) considering Eq. 2	299.5838	817.4542	421.7914
Calculated from the present study using $V_{S25}$ (m/s) considering Eq. 2	317.7776	821.0582	449.746
Calculated from Boore et al. [7] using $V_{S5}$ (m/s)	209.6803	453.9388	281.5558
Calculated from Boore et al. [7] using $V_{S15}$ (m/s)	149.1703	258.7446	192.3064
Calculated from Boore et al. [7] using $V_{S25}$ (m/s)	217.7908	471.5526	294.9737
Calculated from Cadet and Duval [6] using $V_{S5}$ (m/s)	569.9997	1054.129	723.3163

compared to observed. The variability of  $V_{S30}$  for different regions points out the linking of linear amplification with the time-average  $V_S$  to the available depth, which could help in selecting the appropriate estimation of site effect. One thing can also be specified here that IGB soil is less compacted than Japanese and California soil. Hence, using Boore et al. [7] relationships may lead to over estimation of  $V_{S30}$  for IGB region and hence proposed relations are more reliable. Different ways of estimating  $V_{S30}$  using equations proposed in this study are useful where the complete shear wave velocity profile until 30 m is not available. Additionally, in many cases, due to limitation of equipment or site-conditions, it is expensive for low-budget projects to measure velocity profile upto 30 m depth. In these cases,  $V_{S30}$  can be estimated for IGB using the newly proposed regression equations between  $N_z$  and  $V_{S30}$ . Presently, Indian code does have soil-based design spectrum similar to modern codes. Proposed relations are useful design structure as per modern code considering  $V_{S30}$ . Preliminary average values can be obtained from this study to plan detailed subsurface investigation and foundation design for the important study.

## Conclusion

Time average shear wave velocity at 30 m depth ( $V_{S30}$ ) is an essential parameter for site characterization and site amplification estimation. However, still, there is an ongoing debate on whether the estimation of shear wave velocity till 30 m is enough for site amplification for deep sites. Though having limitation,  $V_{S30}$  is still used because of having its reliable and economical estimation. Hence, in this study, a new correlation between  $V_{S30}$  and  $V_{SZ}$  for the entire stretch of IGB has been derived using 275 locations shear wave velocity measurement.

Correlations have been divided into two parts: one where depth is less than 30 m and other being more than 30 m. For depth less than 30 m, second degree polynomial and both linear and orthogonal approach have been used for deriving the correlation. For depth more than 30 m, both linear equation and second degree polynomial equation are used for deriving the correlation. Based on the analysis, it can be concluded that orthogonal linear is predicting better till  $V_{S30} \leq 300$  m/s (Eq. 3) and for  $V_{S30} > 300$  m/s (Eq. 1) orthogonal nonlinear is predicting better. It can be recommended that for correlating  $V_{S30}$  and  $V_{SZ}$  for either  $z$  more than or less than 30 m depth, orthogonal regression analysis can be used for better  $V_{S30}$  prediction. Further, regression relationship between  $V_{S30}$  and  $N_z$ , for  $5 < z < 50$ , has been also developed, for determining  $V_{S30}$  for a site having known SPT-N data at different depths. Further, the distribution  $V_{S30}$  based on  $N_{30}$  for the IGB has been derived. This would be useful in deriving the acceleration response spectrum at different parts of the IGB based on the Indian seismic code. Additionally, depth corresponding to one-quarter of wavelength for various periods for deep profiles of IGB has been determined. Based on the study, it has been concluded that for estimating the amplifications at periods as long as 1 s, the profile must extend at least 100 m in case of IGB. Moreover, velocities known up to 30 m depth are relevant for site amplification at a period less than 1 s, more specifically up to 0.5 s. This study found that existing correlation between  $V_{S30}$  and  $V_{SZ}$  may not be applicable or suitable for the IGB in comparison with the proposed correlations.

**Acknowledgements** The authors thank the Science and Engineering Research Board (SERB) of the Department of Science and Technology (DST), India for funding the project titled “Measurement of shear wave velocity at deep soil sites and site response studies”, Ref: SERB/F/162/2015–2016. Authors also thank Geological Society of

India for providing the Geological and Lithological map required for the study.

## References

- Building Seismic Safety Council (2003) Recommended provisions for seismic regulations for new buildings and other structures, part 1: provisions. Report No. FEMA-450, Federal Emergency Management Agency, Washington, DC
- Eurocode 8 (2004) Design of structures for earthquake resistance, part 1: general rules, seismic actions and rules for buildings, EN 1998-1, European Committee for Standardization (CEN). <http://www.cen.eu/cenorm/homepage.htm>. Accessed Dec 2018
- American Society of Civil Engineers (ASCE) (2010) Minimum design loads for buildings and other structures, standards ASCE/SEI 7-10, ISBN 9780784410851. <http://www.asce.org/Product.aspx?id=2147487569>. Accessed Dec 2018
- Castellaro S, Mulargia F, Rossi PL (2008) VS30: proxy for seismic amplification? *Seismol Res Lett* 79:540–543
- Lee VW, Trifunac MD (2010) Should average shear-wave velocity in the top 30 m of soil be used to describe seismic amplification? *Soil Dyn Earthq Eng* 30:1250–1258
- Cadet H, Duval AM (2009) A shear wave velocity study based on the KiK-net borehole data: a short note. *Seismol Res Lett* 80:440–445
- Boore DM, Thompson EM, Cadet H (2011) Regional correlations of VS30 and velocities averaged over depths less than and greater than 30 meters. *Bull Seismol Soc Am* 6:3046–3059
- Boore DM (2004) Estimating VS30 (or NEHRP site classes) from shallow velocity models (depths < 30 m). *Bull Seismol Soc Am* 94:591–597
- Sun G (2015) Determination of mean shear wave velocity to 30 m depth for site classification using shallow depth shear wave velocity profile in Korea. *Soil Dyn Earthq Eng* 73:17–28
- Anbazhagan P, Sitharam TG (2008) Mapping of average shear wave velocity for bangalore region: a case study. *J Environ Eng Geophys* 13(2):69–84
- Mahajan AK, Mundepi AK, Chauhan N et al (2012) Active seismic and passive micrometer HVSR for assessing site effects in Jammu city, NW Himalaya, India—a case study. *J Appl Geophys* 77:51–62
- Maheshwari U, Boominathan RA, Dodagoudar GR (2010) Seismic site classification and site period mapping of Chennai city using geophysical and geotechnical data. *J Appl Geophys* 72:152–168
- Satyam ND, Rao KS (2008) Seismic site characterization in Delhi region using multi-channel analysis of shear wave velocity (MASW) testing. *Electron J Geotech Eng* 13:167–183
- Anbazhagan P, Kumar A, Sitharam TG (2013) Seismic site classification and correlation between standard penetration test N value and shear wave velocity for Lucknow City in Indo-Gangetic Basin. *Pure appl Geophys* 170:299. <https://doi.org/10.1007/s00024-012-0525-1>
- Govindraju L, Bhattacharya S (2008) Site response studies for seismic hazard analysis for Kolkata city. In: Proceedings of 12th international conference of international association for computer methods and advances in geomechanics, pp 2899–2907
- Hanumantha Rao C, Ramana GV (2009) Site specific ground response analyses at Delhi, India, EJGE, P-16. <http://www.ejge.com/2009/Ppr0936/Ppr0936.pdf>. Last accessed 26th Dec 2014
- Phanikanth VS, Choudhury D, Reddy GR (2011) Equivalent-linear seismic ground response analysis of some typical sites in Mumbai. *Geotech Geol Eng* 29(6):1109–1126
- Shukla J, Choudhury D (2012) Seismic hazard and site-specific ground motion for typical ports of Gujarat. *Nat Hazards* 60(2):541–565
- Desai SS, Choudhury D (2015) Site specific seismic ground response study for Nuclear power plants and ports in Mumbai. *Nat Hazards Rev.* [https://doi.org/10.1061/\(asce\)nh.1527-6996.0000177.04015002](https://doi.org/10.1061/(asce)nh.1527-6996.0000177.04015002)
- BIS 1893 (Part 1) (2016) Indian standard criteria for earthquake resistant design of structures, Sixth Revision, Bureau of Indian Standards, New Delhi
- Singh IB (1996) Geological evolution of Ganga plain—an overview. *J Paleontol Soc India* 41:99–137
- Sastri VV, Bhandari LL, Raju ATR, Dutta AK (1971) Tectonic framework and subsurface stratigraphy of the Ganga Basin. *J Geol Soc India* 12:222–233
- Karunakaran C, Rao R (1979) Status of exploration for hydrocarbons in the Himalayan region-contribution to stratigraphy and structure. *Geol Surv India Publ* 41:1–66
- GSI (Geological Survey of India) (2012) Geological and mineral resources of the states of India 606 Part XV: Punjab and Chandigarh. Govt. of India. ISSN 0579-4706
- Khan IA, Bridge JS, Kappelman J, Wilson R (1997) Evolution of miocene fluvial environments, eastern Potwar plateau, northern Pakistan. *Sedimentology* 44:221–251
- Sahu S, Saha D, Dayal S (2015) Sone megafan: a non-Himalayan megafan of craton origin on the southern margin of the middle Ganga Basin, India. *Geomorphology* 250:349–369
- Bajaj K, Anbazhagan P (2019) Spatial variability of shear wave velocity in the deep and active Indo-Gangetic basin. *Geophys J Int* (under review)
- Bajaj K, Anbazhagan P (2019) Seismic site classification and correlation between V<sub>s</sub> and SPT-N for deep soil sites in Indo-Gangetic basin. *J Appl Geophys* 163:55–72
- Park C, Miller R, Xia J (1998) Imaging dispersion curves of surface waves on multi-channel record. In: Society of exploration geophysicists expanded abstracts, pp 1377–1380
- Xia J, Miller RD, Park CB (1999) Estimation of near-surface shear-wave velocity by inversion of Rayleigh waves. *Geophysics* 64:691–700
- Foti S, Parolai S, Bergamo P, Giulio GD, Maraschini M, Milana G, Picozzi M, Puglia R (2011) Surface wave surveys for seismic site characterization of accelerometric stations in ITACA. *Bull Earthq Eng* 9:1797–1820
- Okada H (2003) The microtremor survey method. *Geophysical monographs series, no. 12.* Society of Exploration Geophysicists
- Park C, Miller R (2008) Roadside passive multichannel analysis of surface waves (MASW). *J Environ Eng Geophys* 13:1–11
- Park CB, Miller RD, Xia J, Ivanov J (2007) Multichannel analysis of surface waves (MASW)-active and passive methods. *Lead Edge* 26:60–64
- Foti S, Comina C, Boiero D, Socco LV (2009) Non-uniqueness in surface-wave inversion and consequences on seismic site response analyses. *Soil Dyn Earthq Eng* 29:982–993
- Anbazhagan P, Bajaj K, Moustafa SSR, Al-Arifi NSN (2019) Acquisition and analysis of surface wave data in the Indo Gangetic Basin. In: Wasowski J, Dijkstra T (eds) Recent research on engineering geology and geological engineering. GeoMEast 2018. Sustainable Civil Infrastructures. Springer, Cham
- Castellaro S, Mulargia F, Rossi PL (2008) Vs30: proxy for seismic amplification? *Seismol Res Lett* 79(4):540–543
- Joyner WB, Warrick RE, Fumal TE (1981) The effect of quaternary alluvium on strong ground motion in the Coyote Lake, California, earthquake of 1979. *Bull Seismol Soc Am* 71:1333–1349
- Day SM (1996) RMS response of a one-dimensional halfspace to SH. *Bull Seismol Soc Am* 96:363–370

40. Boore DM (2003) Prediction of ground motion using the stochastic method. *Pure appl Geophys* 160:635–676
41. Building Seismic Safety Council (BSSC) (2001) NEHRP recommended provisions for seismic regulations for new buildings and other structures—part 1: provisions, FEMA-368; part 2: commentary, FEMA-369. Federal Emergency Management Agency, Washington, DC
42. Anbazhagan P, Parihar A, Rashmi HN (2012) Review of correlations between SPT N and shear modulus: a new correlation applicable to any region. *Soil Dyn Earthq Eng* 36:52–69
43. Selvam LP, Anbazhagan P, Sreenivas M, Akshath HK, Peter J (2013) Indigenous SPT-Hammer Energy measurement apparatus and preliminary studies. 4IYGEC, 1–18 May, Chennai, India
44. Anbazhagan P, Agarwal A, Prakash D (2016) Effect of energy efficiency of hammer on liquefaction potential of soil. In: Indian geotechnical conference (IGC 2016). 15–16 December, Madras, India
45. Bajaj K, and Anbazhagan P (2019) Effective input velocity and deoth for deep and shallow sites for site response analysis using KiK-Net downhole array data. *Natural Hazards* (Under Riview)
46. Anbazhagan P, Prabhu Gajawada, Moustafa Sayed SR, Arifi Al Nassir S, Aditya Parihar (2014) Provisions for geotechnical aspects and soil classification in Indian seismic design code IS-1893. *Disaster Adv* 7(3):72–89

**Publisher's Note** Springer Nature remains neutral with regard to jurisdictional claims in published maps and institutional affiliations.